An Improved Distributed Secondary Control Method for DC Microgrids With Enhanced Dynamic Current Sharing Performance

Panbao Wang, *Member, IEEE*, Xiaonan Lu, *Member, IEEE*, Xu Yang, Wei Wang, *Member, IEEE*, and Dianguo Xu, *Senior Member, IEEE*

***Abstract*—This paper proposes an improved distributed secondary control scheme for dc microgrids (MGs), aiming at overcoming the drawbacks of conventional droop control method. The proposed secondary control scheme can remove the dc voltage deviation and improve the current sharing accuracy by using voltage-shifting and slope-adjusting approaches simultaneously. Meanwhile, the average value of droop coefficients is calculated, and then it is controlled by an additional controller included in the distributed secondary control layer to ensure that each droop coefficient converges at a reasonable value. Hence, by adjusting the droop coefficient, each participating converter has equal output impedance, and the accurate proportional load current sharing can be achieved with different line resistances. Furthermore, the current sharing performance in steady and transient states can be enhanced by using the proposed method. The effectiveness of the proposed method is verified by detailed experimental tests based on a 3 × 1 kW prototype with three interface converters.**

***Index Terms*—Current sharing, dc microgrid (MG), droop control, low-bandwidth communication (LBC), secondary control.**

I. Introduction

With the increasing penetration of renewable energy sources into modern electric grids, the concept of microgrid (MG) has been proposed as an aggregated entity to integrate distributed generators (DGs) and controllable/noncontrollable loads [1]. Since various types of sources and loads in an MG feature dc coupling, e.g., photovoltaic (PV), light emitting diode lighting, etc., it is an efficient way to employ dc MG to collect these units. Compared to ac MGs, dc MGs can shorten the energy conversion chain by reducing the number of dc–ac or ac–dc converters. Meanwhile, they also feature the advantages of higher efficiency, enhanced reliability, lower control complexity, etc. [2]–[5].

A generic low-voltage single-bus dc MG with various sources and loads is depicted in Fig. 1. Among them, when the grid-connected interface inverter is activated, the dc MG can be operated in grid-connected mode to exchange power with the main ac grid. Once the interface inverter is deactivated, the dc MG can be operated in islanded mode to form a local dc-coupled energy system. In such case, the DG units and energy storage are used to sustain the stable operation of the system. The optimal dispatch of energy flow within the system can be achieved by the control system of dc MG. Meanwhile, economic operation and black start process can be realized when necessary [6], [7].

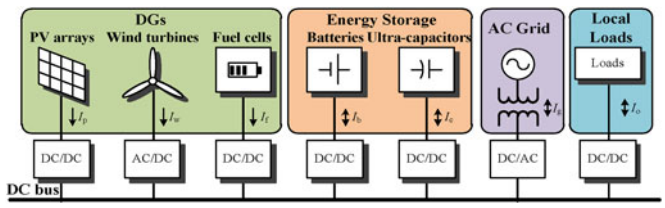

Fig. 1. Generic architecture of low-voltage single-bus dc MGs.

Several centralized, decentralized, distributed, and hierarchical control methods have been proposed to obtain prolonged and reliable operation of dc MGs [8]–[15]. However, due to the fact that the units in dc MGs are connected in parallel to the common dc bus, current sharing among power generation units has become a primary issue. In the earlier studies, current sharing issues have been discussed for parallel-connected converter modules such as input-parallel output-parallel [16] and input-series output-parallel [17] dc–dc converter modules, uninterrupted power supplies [18], distributed power systems (DPSs) [19], [20], etc. The proposed current sharing methods mainly include master-slave control, average current method, droop control, and so on [21].

DC droop control and its variants have been applied in dc MGs for current sharing purpose and have been intensively studied in the past years [2], [6], [9]–[11], [13]–[15]. Similarly to dc DPSs, individual units in dc MGs are dispersedly connected to the common bus. Hence, compared to the master-slave control relying on high bandwidth communication, droop control without interconnecting high bandwidth communication links is more suitable for dc MGs. Furthermore, the application of droop control can also bring advantages such as high reliability and simple expandability to dc MGs [22], [23].

Despite above advantages of droop control, its limitations should be also noticed [24]–[26], [28], [29]. The drawback of the conventional droop control is that the output voltage is linearly reduced with increasing output current, which induces

Manuscript received February 13, 2015; revised April 29, 2015, August 5, 2015, and September 29, 2015; accepted November 3, 2015. Date of publication November 10, 2015; date of current version March 25, 2016. This work was supported by the National Nature Science Foundation of China (51477033). Recommended for publication by Associate Editor S. Mazumder.

P. Wang, X. Yang, W. Wang, and D. Xu are with the Department of Electrical Engineering, Harbin Institute of Technology, Harbin 150001, China (e-mail: wangpanbao@hit.edu.cn; primerxu@aol.com; wangwei602@hit.edu.cn; xudiang@hit.edu.cn).

X. Lu is with the Energy Systems Division, Argonne National Laboratory, Lemont IL 60439 USA (e-mail: xiaonan.lu@anl.gov).

Color versions of one or more of the figures in this paper are available online at http://ieeexplore.ieee.org.

Digital Object Identifier 10.1109/TPEL.2015.2499310

a voltage deviation at the local and common dc buses compared to their rated values. Meanwhile, load distribution in dc MGs is influenced by mismatched line impedances.

In order to solve the aforementioned problems, secondary control [27]–[34] has been proposed to compensate voltage deviation and enhance current sharing accuracy simultaneously. By exchanging information via communication links, secondary control is capable of adjusting the set-points of primary control. The method like this has been also applied in the earlier network-based control of power electronic systems [35]–[37]. A radio frequency communication-based control for interactive power electronics networks was proposed in [36], and the effect of time delay in the system was evaluated. Considering the distributed nature of dc MGs, low bandwidth communication (LBC) is more suitable to be employed for the secondary control diagram, and the LBC networks can be realized by using controllers area network, power line communication, and so on.

The existing secondary control of dc MGs can be summarized into two categories: centralized secondary control and distributed secondary control [27]–[31]. A centralized secondary control diagram is proposed in [27], which means the secondary adjustment is completed in the microgrid central controller (MGCC). In particular, MGCC first samples the real-time value of the common dc bus voltage by using LBC, and then implements secondary control scheme and generates a voltage compensating term to be added into the reference value of the primary control level. As a result, the dc bus voltage is restored. However, the single-point-of-failure should be noticed for centralized secondary control diagram. A distributed secondary control diagram is proposed in [28]. In this method, the secondary control scheme is implemented in the local controllers, and the information used in the local secondary control scheme is exchanged via LBC network. This method can avoid the impact of single-point-of-failure in the centralized secondary control. However, the effect of line resistances has not been comprehensively considered. Moreover, the current sharing accuracy enhancement is only realized by using larger droop coefficients.

In [29], a distributed secondary control scheme that is used to restore dc output voltage and enhance the current sharing accuracy is proposed. Two additional controllers for average dc output voltage and average dc output current are introduced in the secondary control diagram. The control loops are implemented locally, and the voltage restoration and current sharing accuracy enhancement can be achieved simultaneously. However, every converter needs to obtain all the other converters' output voltage and current to calculate the average values. This method can be regarded as static averaging, which is not flexible enough and leads to high communication stress. Consensus algorithm with a sparse communication network is used in [30] and [31] to achieve a distributed secondary control diagram with dynamic averaging, in which only the information from the neighboring converters rather than the global information from all the converters are needed to restore the dc output voltage and enhance current sharing accuracy. By using the consensus algorithm, the flexibility of the system is enhanced and the plug-and-play capability can be provided. Since only the neighboring information is needed, the communication stress is highly reduced.

In [27]–[30], the approaches to compensate the dc-bus voltage and enhance the current sharing accuracy are mainly realized by adding a voltage-shifting value to the droop controller. This means keeping the droop coefficients constant and shifting the droop curves. The steady-state current sharing accuracy of parallel converters can be improved by using closed-loop regulation. However, since fixed droop coefficients are used, the equivalent output impedances, i.e., the sum of droop coefficient and line impedance, are not the same, which results in further regulation of the average current controller under fast-changing load condition. Instead of using voltage-shifting approach, droop coefficient adjustment, namely slope-adjusting method, is employed in [31] to enhance the current sharing accuracy, where single current feedback loop is applied to conduct the adjustment, and the implementation of this control method is relatively complicated. The convergence speed and stability should be further noticed.

In this paper, an improved secondary control method with enhanced dynamic performance under fast-changing load current condition is proposed. In this control method, three compensating controllers are employed, i.e., local average voltage controller, local average current controller, and average droop coefficient controller. The first controller is used to restore the local dc voltage. Hence, the dc voltage deviation induced by droop control can be eliminated. The second and third controllers are employed to work together and regulate the droop coefficient so that the equivalent output impedance of each interface converter can be the same. The average of the droop coefficients is controlled to its reference value to avoid unreasonable selections of the droop coefficients. Although the voltage and current data is exchanged via low bandwidth network, considering the equivalent output impedance that is adjusted to be the same, the proposed secondary control diagram can ensure enhanced dynamic behavior with fast-changing load current.

The system stability of the proposed method is studied by using small-signal analysis. The current sharing performance of the proposed secondary control method is discussed with different communication delays and line impedances. Meanwhile, local and common loads are both taken into account. The experimental verifications are conducted to test both of the steady and dynamic performances of the proposed method, including voltage restoration, current sharing accuracy enhancement, fast load fluctuations, and step change of load current. Furthermore, the resiliency of the proposed algorithm is examined when encountering converter failures. It should be noted that considering the requirement of low-cost implementation of the control systems in the industrial converters, micro-controller units (MCUs) are used in the prototype. Meanwhile, the LBC is used as the communication system. It can be demonstrated that the proposed secondary control diagram can be effectively implemented by using this low-cost combination.

The rest of the paper is organized as follows. In Section II, the centralized and distributed secondary control methods along with droop control in the primary control level are reviewed and discussed. Section III analyzes the current sharing accuracy with

voltage-shifting-based secondary control under fast-changing load current condition. Section IV introduces the principle of the proposed secondary control scheme and discusses the system stability by using small-signal analysis. Section V shows the detailed experimental results and the comparison of the proposed method and the existing voltage-shifting secondary control method. Finally, Section VI summarizes the paper and draws the conclusion.

II. Review of Secondary Control Schemes of DC MGs

In dc MGs, dc voltage deviation is induced when the droop control is used to achieve load current sharing among parallel interface converters [38]–[40]. Meanwhile, the current sharing accuracy is degraded with mismatched line impedances [29]. Generally, the larger droop coefficients can be used to enhance the current sharing accuracy. However, in this case, the dc voltage can further deviate from its reference value. Hence, secondary control schemes should be employed to overcome these drawbacks of the conventional droop control method.

As shown in Fig. 2(a), a basic secondary compensator is presented in [27], in which a voltage control loop adjusting dc bus voltage is included in the MGCC. The dc bus voltage is obtained from a remote voltage sensor, and the secondary control signals are sent from the MGCC to the interface converters through LBC network. Primary control loops of each converter are comprised of inner voltage and current loops and droop control.

The droop control method with the above secondary control scheme in [27] is shown as

$$v_{\mathrm{dc}i}^{*} = v_{\mathrm{dc}}^{*} - r_{di} i_{\mathrm{dc}i} + \underbrace{\left(k_p + \frac{k_i}{s}\right)\left(v_{\mathrm{dc}}^{*} - v_{\mathrm{dcbus}}\right)}_{\text{Voltage-Shifting Term}} \quad (1)$$

where v_{dc}^{*} is the given voltage reference value of dc bus, $v_{\mathrm{dc}i}^{*}$ is the given voltage reference value of converter #*i*, $r_{\mathrm{d}i}$ is the droop coefficient of converter #*i*, $i_{\mathrm{dc}i}$ is the output current of converter #*i*, v_{dcbus} is the voltage of common dc bus at the point-of-common-coupling (PCC), k_p and k_i are the proportional and integral terms of the secondary controller for voltage restoration.

It can be seen from (1) that the secondary control method in [27] can be regarded as a voltage-shifting-based method.

A distributed secondary control framework is proposed in [28]. It should be noted that distributed control here represents the control diagram that only relies on local controller and no central controller is required. Compared to the centralized secondary control method, the secondary control scheme implemented in the local controller can effectively avoid the single-point-of-failure caused by the malfunction of the central controller. The output current of each converter is exchanged via LBC, and the average current is calculated in the local controllers to be multiplied by a coefficient and sent to the droop controller. This method is equivalent to add a linearly compensating term into the reference of the conventional droop controller, and it is effective to restore the dc voltage. However, the current sharing accuracy can be only achieved by selecting large droop coefficients. When the line impedances are highly mismatched, current sharing accuracy will be further degraded. The

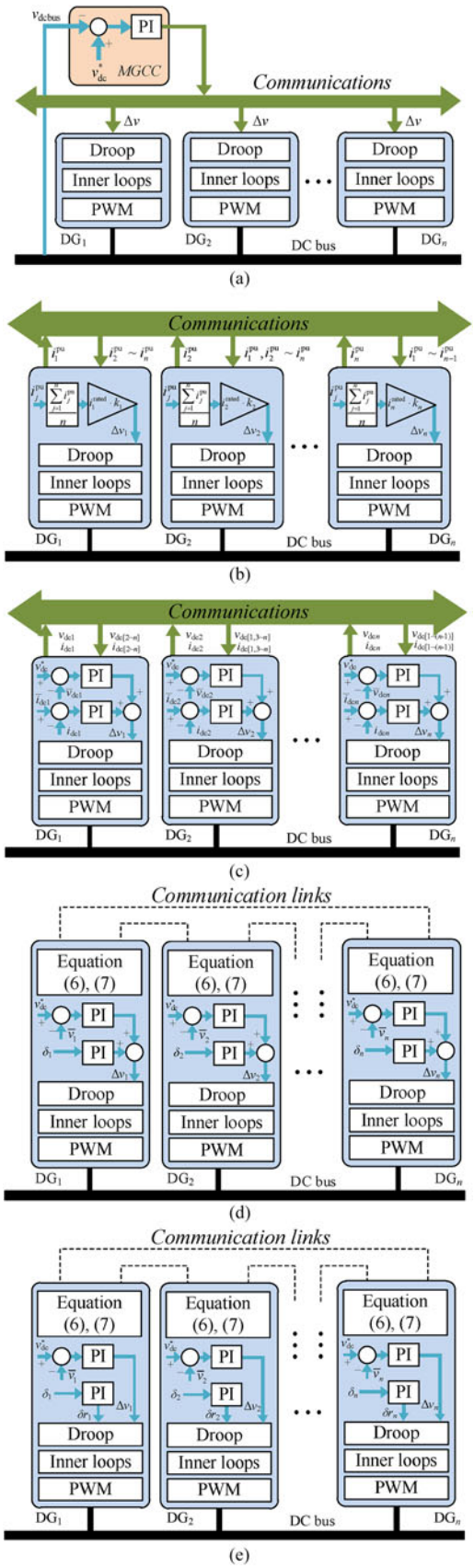

Fig. 2. Control diagrams of the existing secondary control methods for dc MGs. (a) Proposed in [27]. (b) Proposed in [28]. (c) Proposed in [29]. (d) Proposed in [30]. (e) Proposed in [31].

droop expression used in this method with the voltage-shifting term derived from the secondary controller can be shown as

$$v_{\mathrm{dc}i}^{*} = v_{\mathrm{dc}}^{*} - r_{\mathrm{d}i} i_{\mathrm{dc}i} + \underbrace{k_j \cdot i_j^{\mathrm{avg}} \cdot i_j^{\mathrm{rated}}}_{\text{Voltage-Shifting Term}} \tag{2}$$

where i_j^{avg} in per-unit value is the average current of system, k_j and i_j^{rated} are the shift gain and rated current of converter #*j*, respectively.

An average voltage controller and an average current controller are added in the secondary control level to restore the dc bus voltage and enhance the current sharing accuracy simultaneously in [29]. These two additional controllers are also implemented in the local controller. As shown in Fig. 2(c), the average values of dc voltage and current are calculated and sent back to compare with the voltage reference value and local output current. Two proportional-integral (PI) controllers for average voltage and average current respectively are employed, and their output values are added into the droop controller. The expression of the droop control method in [29] is shown as

$$v_{\mathrm{dc}i}^{*} = v_{\mathrm{dc}}^{*} - r_{\mathrm{d}i} i_{\mathrm{dc}i} + \underbrace{\left(k_{\mathrm{pv}} + \frac{k_{iv}}{s}\right)\left(v_{\mathrm{dc}}^{*} - \bar{v}_{\mathrm{dc}i}\right) - \left(k_{pc} + \frac{k_{ic}}{s}\right)\left(i_{\mathrm{dc}i} - \bar{i}_{\mathrm{dc}i}\right)}_{\text{Voltage-ShiftingTerm}} \tag{3}$$

where $i_{\mathrm{dc}i}$ is the output current of converter #*i*, $\bar{v}_{\mathrm{dc}i}$ and $\bar{i}_{\mathrm{dc}i}$ are the calculated average value of output voltages and currents in converter #*i*, $k_{\mathrm{pv}}, k_{\mathrm{iv}}$ and $k_{\mathrm{pc}}, k_{\mathrm{ic}}$ are the parameters of the voltage and current regulators. Note that the currents depicted in Fig. 2(c) are per-unit values, and the real output current value of each converter depends on its power rating.

By considering the secondary control diagrams in [27]–[29], it can be seen from (1)–(3) that they can be categorized as voltage-shifting methods, in which the compensating terms generated by the secondary control level are added into the conventional droop controller as voltage-shifting corrections.

In [30] and [31], a sparse communication network is employed to realize distributed secondary control of dc MGs. In this method, every converter only needs to communicate with its neighbors, and consensus algorithm is employed to achieve dynamic averaging. The obtained data is sent to the secondary control level to carry out voltage and current regulation. As shown in Fig. 2(d), the secondary control used in [30] is achieved in local controller as a distributed control method. It should be noted that, as similar to [27]–[29], fixed droop coefficients are used in [30]. The droop control method with the above secondary control scheme in [30] is shown as

$$v_{\mathrm{dc}i}^{*} = v_{\mathrm{dc}}^{*} - r_{\mathrm{d}i} i_{\mathrm{dc}i} + \underbrace{\left(k_{\mathrm{pv}} + \frac{k_{iv}}{s}\right)\left(v_{\mathrm{dc}}^{*} - \bar{v}_i\right) + \left(k_{pc} + \frac{k_{ic}}{s}\right)\delta_i}_{\text{Voltage-Shifting Term}} \tag{4}$$

where $\bar{v}_i$ is the average voltage of participating interface converters, δ_i is the mismatched current.

In regard to the secondary control method proposed in [31], as shown in Fig. 2(e), the dc voltage is restored by using voltage-shifting compensating term. Meanwhile, the current mismatch induced by unequal line impedances is coped with by dynamically adjusting the droop coefficient. The droop control method with the above secondary control scheme in [31] is shown as

$$v_{\mathrm{dc}i}^{*} = v_{\mathrm{dc}}^{*} - \underbrace{\left(r_{i0} - \left(k_{pr} + \frac{k_{ir}}{s}\right)\delta_i\right)}_{\text{Slope-Adjusting Term}} i_{\mathrm{dc}i} + \underbrace{\left(k_{\mathrm{pv}} + \frac{k_{iv}}{s}\right)\left(v_{\mathrm{dc}}^{*} - \bar{v}_i\right)}_{\text{Voltage–Shifting Term}} \tag{5}$$

where r_{i0} is the initial droop coefficient of converter #*i*, δ_i is the current mismatch value, k_{pr} and k_{ir} are the proportional and integral terms of the secondary controller for droop coefficient adjustment.

The average voltage of system using dynamic consensus protocol in [30] and [31] can be expressed as follows:

$$\bar{v}_i(t) = v_i(t) + \int_0^t \sum_{j \in N_i} a_{ij}\left(\bar{v}_j(\tau) - \bar{v}_i(\tau)\right) d\tau \tag{6}$$

where v_i is the sample voltage of local converter, $\bar{v}_j$ is the estimated average voltage of neighboring converter, and a_{ij} is the communication weight.

Current mismatch in the system can be expressed as follows [30], [31]:

$$\delta_i = \sum_{j \in N_i} b a_{ij}\left(i_j^{pu} - i_i^{pu}\right) \tag{7}$$

where i_i^{pu} and i_j^{pu} are per-unit currents of local converter and neighboring converters, *b* is a coupling coefficient.

It should be noted that, as shown in (4), the secondary control in [30] can be also categorized as a voltage-shifting method since it is realized by adding compensating term in the conventional droop controller. For the secondary control in [31], it can be regarded as a hybrid method with both voltage-shifting and slope-adjusting methods. In particular, besides adding a compensating term for dc voltage restoration, the slope of the droop curve, i.e., the droop coefficient, is adjusted to enhance the current sharing accuracy by using the dynamic average current controller.

By using the above analysis and comparison, the existing secondary control methods in dc MG can be summarized, as shown in Table I. In terms of control architecture, centralized control is employed in [27], while distributed control is used in [28]–[31]. Meanwhile, static averaging is utilized in [28] and [29], and since consensus algorithm is adopted, dynamic averaging is realized in [30] and [31]. In terms of compensating strategy, voltage-shifting approach is used in all the above secondary control schemes, while slope-adjusting method is used in [31] to achieve adaptive droop coefficient.

TABLE I
COMPARISON OF EXISTING SECONDARY CONTROL METHODS

Secondary control methods	Control Architecture				
	Centralized Control	Distributed Control		Compensating Strategy	
		Static Averaging	Dynamic Averaging	Voltage Shifting	Slope Adjusting
Guerrero et al. [27]	√			√	
Anand et al. [28]		√		√	
Lu et al. [29]		√		√	
Nasirian et al. [30]			√	√	
Nasirian et al. [31]			√	√	√

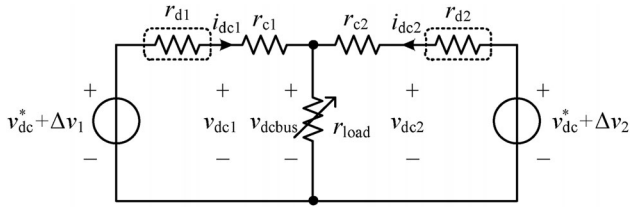

Fig. 3. Equivalent circuit of dc MG with two terminals.

III. CURRENT SHARING ANALYSIS WITH FAST-CHANGING LOAD CURRENT

As presented in Section II, by using the secondary control method incorporating additional controllers for average dc voltage and average dc current, the current sharing accuracy can be enhanced. However, since the droop coefficients are fixed, with mismatched line impedance, the equivalent output impedance of each interface converter, i.e., the sum of droop coefficient and line impedance, is different from each other. When the load current changes rapidly, in order to maintain the required current sharing proportion, the average dc current controller needs to further regulate the output current since the equivalent output impedances are still unequal. Hence, the dynamic performance with fast-changing load current is degraded. The reason for the above drawback is analyzed below by using the equivalent circuit model.

The equivalent circuit of voltage-shifting based secondary control is shown in Fig. 3, r_{c1}, r_{c2} are the line impedances, r_{d1}, r_{d2} are virtual impedances that equal to the droop coefficients, and $v_{\rm dc1}, v_{\rm dc2}, i_{\rm dc1}, i_{\rm dc2}$ are the dc voltage and current at the output sides of converters. In addition, Δv_1 and Δv_2 are the voltage-shifting values of the two converters which can be obtained by (3).

By analyzing the circuit in Fig. 3, it can be derived that:

$$v_{\rm dcbus} = \frac{g_1}{g_1+g_2+g_{\rm load}} \cdot v_{\rm dc1}^* + \frac{g_2}{g_1+g_2+g_{\rm load}} \cdot v_{\rm dc2}^* \tag{8}$$

where $g_i = 1/(r_{ci}+r_{\rm di})$, $g_{\rm load} = 1/r_{\rm load}$, $v_{\rm dci}^* = v_{\rm dc}^* + \Delta v_i$, $i = 1, 2$.

Hence, the output current can be achieved as

$$i_{\rm dc1} = \frac{g_1[(g_2+g_{\rm load})\cdot v_{\rm dc1}^* - g_2 \cdot v_{\rm dc2}^*]}{g_1+g_2+g_{\rm load}} \tag{9}$$

$$i_{\rm dc2} = \frac{g_2[(g_1+g_{\rm load})\cdot v_{\rm dc2}^* - g_1 \cdot v_{\rm dc1}^*]}{g_1+g_2+g_{\rm load}}. \tag{10}$$

The difference between $i_{\rm dc1}$ and $i_{\rm dc2}$ can be thereby calculated as

$$\Delta i_{\rm dc} = i_{\rm dc1} - i_{\rm dc2} = \frac{2(v_{\rm dc1}^* - v_{\rm dc2}^*)r_{\rm load} + [(r_{c2}+r_{d2})v_{\rm dc1}^* - (r_{c1}+r_{d1})v_{\rm dc2}^*]}{(r_{c1}+r_{d1}+r_{c2}+r_{d2})r_{\rm load} + (r_{c1}+r_{d1})(r_{c2}+r_{d2})}. \tag{11}$$

In order to study the impact of load variation, the derivative $\frac{d\Delta i_{\rm dc}}{dr_{\rm load}}$ is obtained as below

$$\frac{d\Delta i_{\rm dc}}{dr_{\rm load}} = \frac{(r_{c1}+r_{d1}-r_{c2}-r_{d2})[(r_{c2}+r_{d2})v_{\rm dc1}^* + (r_{c1}+r_{d1})v_{\rm dc2}^*]}{[(r_{c1}+r_{d1}+r_{c2}+r_{d2})r_{\rm load} + (r_{c1}+r_{d1})(r_{c2}+r_{d2})]^2}. \tag{12}$$

It can be concluded from (12) that, if and only if $r_{c1}+r_{d1} = r_{c2}+r_{d2}$, i.e., the equivalent output impedances of the interface converters are equal to each other, $\Delta i_{\rm dc}$ has the minimized influence imposed by the load variation. Hence, when the current sharing error is eliminated by the secondary control diagram, as long as the equivalent output impedances are kept equal, the current sharing accuracy can be ensured even though the load current changes rapidly.

IV. PROPOSED SECONDARY CONTROL SCHEME

As analyzed in Section III, the voltage-shifting based secondary control cannot change the equivalent output impedance of the converters. When the equivalent output impedances are not equal to each other and the communication speed is not fast enough, a certain period of time is needed for the average current controller to regulate the dc output current with fast-changing load current. Especially when the difference of line impedances is relatively large, the dynamic current sharing effect of secondary control based on fixed droop coefficients will be further degraded. Hence, a hybrid method with both voltage-shifting and slope-adjusting approaches is proposed in this study. Three additional compensating controllers are added in the distributed secondary control diagram to restore the dc voltage and equalize the equivalent output impedance so that the dynamic load sharing performance can be enhanced. The detailed principle of this method is shown below.

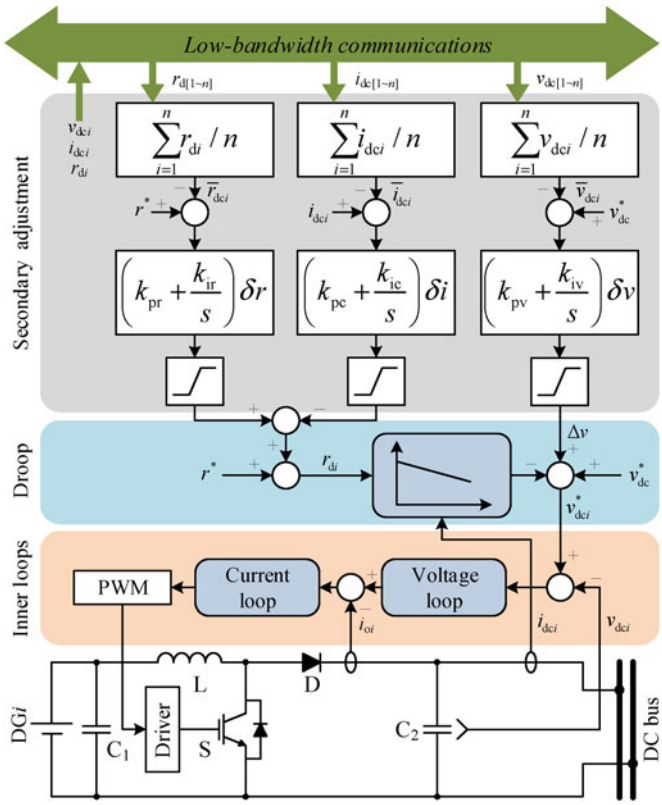

Fig. 4. Control diagram of the proposed control scheme.

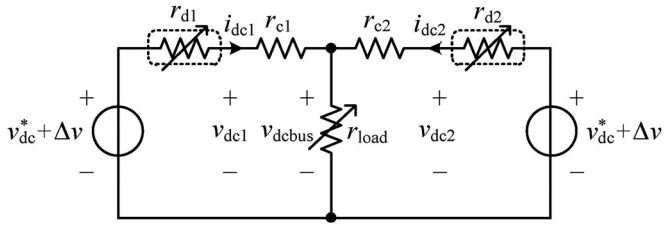

Fig. 5. Equivalent circuit of the proposed secondary control method.

A. Principle of the Proposed Secondary Control Method

In this paper, a distributed secondary control scheme is proposed by using voltage-shifting and slope-adjusting methods simultaneously. In particular, voltage-shifting method is employed to eliminate the voltage deviation induced by droop control, and slope-adjusting method is utilized to adapt the droop coefficient of each converter and achieve equal equivalent output impedance of each interface converter. Hence, fast current sharing can be realized. However, if only adapting the droop coefficients by using the average current compensating controller, multiple combinations of droop coefficients can be achieved. In other words, the droop coefficients can differ from the initial value to a large extend. Therefore, a third compensating controller, i.e., the average droop coefficient controller, is involved in the proposed secondary control scheme. By using the average droop coefficient controller, an additional constraint is employed to avoid the uncertain droop coefficients. Particularly, the droop coefficient is exchanged among different interface converters via the LBC network, and the average value of the droop coefficients is controlled to be its reference value in the local controller. In order to avoid the unacceptable droop coefficients that are either too large or too small, saturation units are also employed to limit the output value of the average droop coefficient controller.

Based on the above analysis, the proposed secondary control scheme for droop-controlled dc MGs can be achieved, as shown in Fig. 4. Without the loss of generality, boost converters are employed as the dc–dc interfaces. The control scheme is comprised of inner-loop controllers, droop controller, and secondary controller. The inner-loop controller is comprised of voltage and current controllers, which is used to control the local dc output voltage of each converter. The reference value of the inner-loop dc voltage controller is generated by the droop controller. Meanwhile, the secondary controller in the local control diagram is comprised of data transceiver modules, average value calculation for voltage, current and droop coefficient, and three compensating PI controllers. The average voltage controller compensates the output voltage deviation, and produces a voltage-shifting value which is added to the output value of the droop controller. The output of average current controller and average droop coefficient controller are used to adjust the local droop coefficient, i.e., the slope of the droop curve. As a result, by using the compensating controllers for average current and droop coefficient, the equivalent output impedance of each converter is controlled to be the same and the average value of droop coefficients is adjusted to its reference value. Hence, the current sharing accuracy can be enhanced.

The adjustment of droop coefficient can be expressed as follows:

$$r_{\mathrm{d}i} = r^* + \left(k_{pr} + \frac{k_{ir}}{s}\right)(r^* - \bar{r}_{\mathrm{dc}i}) - \left(k_{pc} + \frac{k_{ic}}{s}\right)(i_{\mathrm{dc}i} - \bar{i}_{\mathrm{dc}i}) \tag{13}$$

where r^* is the given reference value of droop coefficient, $\bar{r}_{\mathrm{dc}i}$ is the calculated average value of droop coefficients in converter #i, $k_{\mathrm{pr}}, k_{\mathrm{ir}}$ and $k_{\mathrm{pc}}, k_{\mathrm{ic}}$ are the control parameters of the average droop coefficient and average current regulators.

The whole secondary control loops can be derived below

$$v^*_{\mathrm{dc}i} = v^*_{\mathrm{dc}} - \underbrace{(r^* + G_{pir}\,(r_{\mathrm{ref}} - \bar{r}_{\mathrm{dc}i}) - G_{pic}\,(i_{\mathrm{dc}i} - \bar{i}_{\mathrm{dc}i}))}_{\text{Slope-Adjusting Term}} \cdot i_{\mathrm{dc}i} + \underbrace{G_{piv}\,(s) \cdot (v^*_{\mathrm{dc}} - \bar{v}_{\mathrm{dc}i})}_{\text{Voltage-Shifting Term}} \tag{14}$$

where $G_{\mathrm{piv}}(s), G_{\mathrm{pir}}(s)$, and $G_{\mathrm{pic}}(s)$ are transfer functions of the average voltage, average droop coefficient, and average current regulators, respectively.

The equivalent circuit of the proposed method is depicted in Fig. 5. Here, two converters connected in parallel with the same capacity are selected as an example. In Fig. 5, r_{c1}, r_{c2} are the line impedances, r_{d1}, r_{d2} are virtual impedances that are equal to the droop coefficients, and $v_{\mathrm{dc}1}, v_{\mathrm{dc}2}, i_{\mathrm{dc}1}, i_{\mathrm{dc}2}$ are

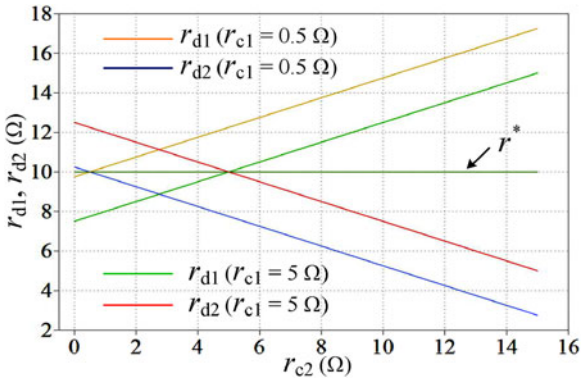

Fig. 6. Droop curves adaption with different line impedances.

the voltage and current values at the output sides of converters. Meanwhile, Δv is the droop shifting values of two converters.

As shown in Fig. 5, the proposed method enhances current sharing accuracy by adapting r_{d1}, r_{d2} together with voltage-shifting method. In other words, voltage restoration and current sharing accuracy enhancement are implemented by shifting droop curve and adjusting the slope of the droop curve simultaneously in this method.

Since PI controllers are used for the average current and average droop coefficient, the steady-state relationships of $r_{d1}, r_{d2}, r_{c1}, r_{c2}$, and $i_{\mathrm{dc}1}, i_{\mathrm{dc}2}$ can be obtained as follows:

$$i_{\mathrm{dc}1} \approx i_{\mathrm{dc}2} \tag{15}$$

$$(r_{d1} + r_{d2})/2 \approx r^*. \tag{16}$$

Considering the main power circuit in Fig. 5, it is derived

$$(v_{\mathrm{dc}}^* + \Delta v) - (r_{d1} + r_{c1})\, i_{\mathrm{dc}1} = (v_{\mathrm{dc}}^* + \Delta v) - (r_{d2} + r_{c2})\, i_{\mathrm{dc}2}. \tag{17}$$

Substituting (15) into (17), it yields

$$r_{d1} + r_{c1} \approx r_{d2} + r_{c2}. \tag{18}$$

It can be seen from (18) that the equivalent output impedance of each converter reaches the same value after the secondary control diagram with three compensating controllers is activated. Since the equivalent output impedance keeps the same with load current variation, the current sharing accuracy in both steady and transient state can be guaranteed.

Combining (16) and (18), it is calculated that

$$\begin{cases} r_{d1} \approx r^* + \dfrac{r_{c2} - r_{c1}}{2} \\ r_{d2} \approx r^* + \dfrac{r_{c1} - r_{c2}}{2} \end{cases}. \tag{19}$$

It can be seen that different droop coefficients corresponding to the different line impedances can be obtained from (19). For example, as shown in Fig. 6, the line impedance r_{c1} is equal to 0.5 or 5 Ω and the reference value of droop coefficient r^* is set to 10 Ω. When the line impedance r_{c2} changes, the values of r_{d1} and r_{d2} change accordingly.

It can be seen from Fig. 6 that when the line impedances of the two converters are the same, droop coefficients of both converters will be equal to the setting value; when the line impedances are different, the droop coefficients of the converters are adjusted adaptively to make the equivalent output impedances equal to each other. Eventually, it can be ensured that the average value of the droop coefficients is equal to the setting value.

It should be noted that (19) is used here only to show the corresponding changes of the droop coefficient and the line impedance. In the control diagram, the droop coefficient converges at these theoretical values by using the additional average droop coefficient and average output current controllers in the proposed secondary control level, as shown in (13).

B. Stability Analysis of the Proposed Secondary Control Method

Stability analysis of the proposed control diagram in Fig. 4 is conducted in this section. Without loss of generality, a dc MG with two terminals is selected as an example here. It can be seen that three compensating controllers are employed in the improved secondary control layer, i.e., local average voltage controller, local average current controller, and average droop coefficient controller. The outputs of these three controllers are synthesized in the conventional droop controller to generate the reference value of the local dc voltage, so that the additional control objectives can be achieved. In particular, the reference value of local dc voltage is derived as

$$v_{\mathrm{dc}i}^* = v_{\mathrm{dc}}^* + \left[k_{\mathrm{pv}}\left(v_{\mathrm{dc}}^* - \bar{v}_{\mathrm{dc}i}\right) + k_{iv}\int\left(v_{\mathrm{dc}}^* - \bar{v}_{\mathrm{dc}i}\right)dt\right] - i_{\mathrm{dc}i} r_{\mathrm{d}i} \tag{20}$$

where $v_{\mathrm{dc}i}^*$ is the reference value of the local dc output voltage, v_{dc}^* is the rated dc voltage, k_{pv} and k_{iv} are the parameters of the PI compensating controller for the local dc voltage, $\bar{v}_{\mathrm{dc}i}$ is the average value of the dc output voltage, $i_{\mathrm{dc}i}$ is the local dc output current, and $r_{\mathrm{d}i}$ is the droop coefficient.

Since the droop coefficient $r_{\mathrm{d}i}$ in (20) is realized by using the additional PI compensating controllers, it is calculated as

$$r_{\mathrm{d}i} = \left[r^* + k_{pr}\left(r^* - \bar{r}_{\mathrm{dc}i}\right) + k_{ir}\int\left(r^* - \bar{r}_{\mathrm{dc}i}\right)dt\right] - \left[k_{pc}\left(\frac{i_{\mathrm{dc}i}}{k_i} - \bar{i}_{\mathrm{dc}i}\right) + k_{ic}\int\left(\frac{i_{\mathrm{dc}i}}{k_i} - \bar{i}_{\mathrm{dc}i}\right)dt\right] \tag{21}$$

where r^* is the reference value of the droop coefficient, $\bar{r}_{\mathrm{dc}i}$ is the average value of the droop coefficients, k_{pr} and k_{ir} are the parameters of the PI compensating controller for the droop coefficients, k_{pc} and k_{ic} are the parameters of the PI compensating controller for the local dc output current, k_i is the current sharing proportion, $\bar{i}_{\mathrm{dc}i}$ is the average value of the local dc output current.

The reference value of the local dc output voltage can be derived by combining (20) and (21). By performing the small-signal analysis for (20) and (21) and transferring the results into

frequency domain, it yields that

$$\hat{v}^*_{\mathrm{dc}i} = \hat{v}^*_{\mathrm{dc}} + G_{piv}\left(-\hat{\bar{v}}_{\mathrm{dc}i}\right) - I_{\mathrm{dc}i}\hat{r}_{\mathrm{d}i} - R_i\hat{i}_{\mathrm{dc}i} \tag{22}$$

$$\hat{r}_{\mathrm{d}i} = G_{pir}\left(-\hat{\bar{r}}_{\mathrm{dc}i}\right) - G_{pic}\left(\frac{\hat{i}_{\mathrm{dc}i}}{k_i} - \hat{\bar{i}}_{\mathrm{dc}i}\right) \tag{23}$$

where the variables with ^ at the head represent the small-signal terms, the capital letters represent the values of the variables in the steady state, and $G_{\mathrm{piv}}, G_{\mathrm{pic}}$, and G_{pir} represent the PI controllers for the local dc voltage, dc current, and droop coefficient.

Since a dc MG with two terminals is selected as an example, by substituting (22) into (23) and setting i equals 1 and 2, it is obtained that

$$\begin{cases} \hat{v}^*_{\mathrm{dc}1} = \hat{v}^*_{\mathrm{dc}} - G_{piv}\hat{\bar{v}}_{\mathrm{dc}1} + \left(\frac{I_{\mathrm{dc}1}G_{pic}}{k_1} - R_1\right)\hat{i}_{\mathrm{dc}1} \\ \qquad + I_{\mathrm{dc}1}G_{pir}\hat{\bar{r}}_{\mathrm{dc}1} - I_{\mathrm{dc}1}G_{pic}\hat{\bar{i}}_{\mathrm{dc}1} \\ \hat{v}^*_{\mathrm{dc}2} = \hat{v}^*_{\mathrm{dc}} - G_{piv}\hat{\bar{v}}_{\mathrm{dc}2} + \left(\frac{I_{\mathrm{dc}2}G_{pic}}{k_2} - R_2\right)\hat{i}_{\mathrm{dc}2} \\ \qquad + I_{\mathrm{dc}2}G_{pir}\hat{\bar{r}}_{\mathrm{dc}2} - I_{\mathrm{dc}2}G_{pic}\hat{\bar{i}}_{\mathrm{dc}2} \end{cases}. \tag{24}$$

The average dc voltage, dc current, and droop coefficient can be reached as

$$\begin{cases} \hat{\bar{v}}_{\mathrm{dc}1} = \left(\hat{v}_{\mathrm{dc}1} + G_d \cdot \hat{v}_{\mathrm{dc}2}\right)/2 \\ \hat{\bar{v}}_{\mathrm{dc}2} = \left(G_d \cdot \hat{v}_{\mathrm{dc}1} + \hat{v}_{\mathrm{dc}2}\right)/2 \end{cases} \tag{25}$$

$$\begin{cases} \hat{\bar{i}}_{\mathrm{dc}1} = \left(\hat{i}_{\mathrm{dc}1} + G_d \cdot \hat{i}_{\mathrm{dc}2}\right)/2 \\ \hat{\bar{i}}_{\mathrm{dc}2} = \left(G_d \cdot \hat{i}_{\mathrm{dc}1} + \hat{i}_{\mathrm{dc}2}\right)/2 \end{cases} \tag{26}$$

$$\begin{cases} \hat{\bar{r}}_{\mathrm{dc}1} = \left(\hat{r}_{\mathrm{dc}1} + G_d \cdot \hat{r}_{\mathrm{dc}2}\right)/2 \\ \hat{\bar{r}}_{\mathrm{dc}2} = \left(G_d \cdot \hat{r}_{\mathrm{dc}1} + \hat{r}_{\mathrm{dc}2}\right)/2 \end{cases} \tag{27}$$

where G_d models the delay of the LBC network, which is shown as

$$G_d = \frac{1}{1 + \tau \cdot s} \tag{28}$$

where τ is the communication delay.

Considering the configuration of a dc MG with two terminals, it can be derived [29]

$$\begin{cases} i_{\mathrm{dc}1} = \alpha_1 \cdot v_{\mathrm{dc}1} - \lambda \cdot v_{\mathrm{dc}2} \\ i_{\mathrm{dc}2} = \alpha_2 \cdot v_{\mathrm{dc}2} - \lambda \cdot v_{\mathrm{dc}1} \end{cases} \tag{29}$$

where the coefficients α_1, α_2 and λ are calculated as

$$\begin{aligned} \alpha_1 &= \frac{r_{c2} + r_{\mathrm{load}}}{r_{c1}r_{c2} + r_{c1}r_{\mathrm{load}} + r_{c2}r_{\mathrm{load}}} \\ \alpha_2 &= \frac{r_{c1} + r_{\mathrm{load}}}{r_{c1}r_{c2} + r_{c1}r_{\mathrm{load}} + r_{c2}r_{\mathrm{load}}} \\ \lambda &= \frac{r_{\mathrm{load}}}{r_{c1}r_{c2} + r_{c1}r_{\mathrm{load}} + r_{c2}r_{\mathrm{load}}}. \end{aligned} \tag{30}$$

In (30), r_{c1} and r_{c2} represent the line resistance for terminal #1 and #2, and r_{load} represents the load resistance.

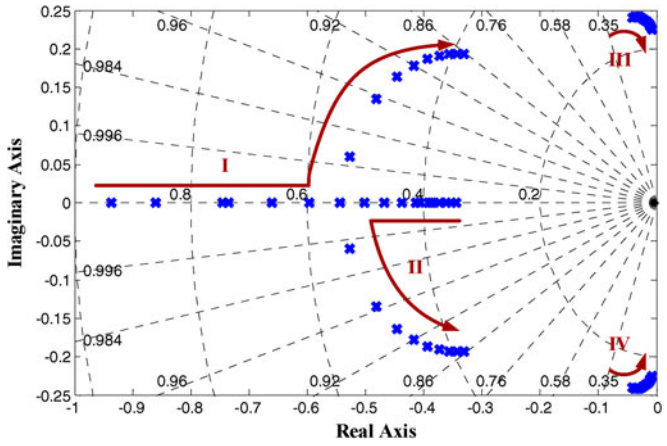

Fig. 7. Dominant poles of the small signal model with different communication delays.

Meanwhile, considering the inner-loop dc voltage and current control loops, it is reached that

$$\hat{v}^*_{\mathrm{dc}i} \cdot \frac{G_{v\_\mathrm{in}}G_{c\_\mathrm{in}}}{1 + G_{v\_\mathrm{in}}G_{c\_\mathrm{in}}} = \hat{v}_{\mathrm{dc}i}, i = 1, 2 \tag{31}$$

where G_{v_in} and G_{c_in} represent the inner-loop voltage and current controllers, respectively.

By transferring (29) and (30) into small-signal expressions and combining the results with (24)–(28) and (31), the following expression can be derived:

$$\hat{v}_{\mathrm{dc}i} = g_i\left(\hat{v}^*_{\mathrm{dc}}, \hat{r}_{d1}, \hat{r}_{d2}\right), i = 1, 2 \tag{32}$$

where g_i shows the relationship of $\hat{v}_{\mathrm{dc}i}/\hat{v}^*_{\mathrm{dc}}$, $\hat{v}_{\mathrm{dc}i}/\hat{r}_{d1}$, and $\hat{v}_{\mathrm{dc}i}/\hat{r}_{d2}$, respectively.

By using the m-script and symbolic toolbox in MATLAB, (32) can be automatically solved and $\hat{v}_{\mathrm{dc}i}/\hat{v}^*_{\mathrm{dc}}$ is selected as an example to test the positions of the dominant poles of the illustrative system. As shown in Fig. 7, when the communication delay changes from 0 to 3 s, the dominant poles of the system move following the traces accordingly. In particular, four dominant poles coexist in the frequency domain analysis result. With increasing communication delay, the dominant poles moves toward the imaginary axis, which challenges the system stability. However, in a wide range of communication delays, all the dominant poles locate in the left half of s domain. Hence, the system stability can be guaranteed.

C. *Voltage-Shifting Equalization*

As presented in Section I, comparative study about dynamic effect between centralized and distributed secondary control is carried out in [32]. Additionally, distributed secondary control is verified to have better robustness than centralized method. Hence, distributed secondary control framework is employed in this paper, and the aforementioned secondary regulation algorithms are implemented in the local controllers. However, in the course of voltage restoration with distributed secondary control, deviations would occur to the voltage adjustment, which may

lead to poor dynamic effect of current sharing. Following is the detailed analysis.

In the equivalent circuit of the proposed secondary control as shown in Fig. 5, before secondary control is activated, voltages v_1 and v_2 can be represented as follows:

$$\begin{cases} v_{\rm dc1} = v_{\rm dcbus} + r_{c1} \cdot i_{\rm dc1} = v_{\rm dc}^* - r_{d1} \cdot i_{\rm dc1} \\ v_{\rm dc2} = v_{\rm dcbus} + r_{c2} \cdot i_{\rm dc2} = v_{\rm dc}^* - r_{d2} \cdot i_{\rm dc2} \end{cases}. \tag{33}$$

As can be seen, under the circumstances of different line impedances and unbalanced output currents, $v_{\rm dc1}$ and $v_{\rm dc2}$ are not equal. If the voltage restoration is implemented by distributed secondary control on this occasion, there will be slight deviation on voltage-shifting value of each converter due to the different sampled voltages $v_{\rm dc1}$ and $v_{\rm dc2}$. This difference induces the change of droop coefficients during current sharing regulation and leads to mismatched equivalent output impedance. The inequality is similar to the phenomenon caused by voltage-shifting secondary control method, and ultimately results in unsatisfied dynamic current sharing performance.

In order to realize voltage restoration by distributed secondary control and ensure equivalent voltage-shifting amounts at the same time, an equalization method is adopted in this secondary control scheme. Specifically, the average value of voltage-shifting amounts of converters is calculated in every communication cycle. Then the value is sent to the average voltage regulator of the converters as a new voltage-shifting value. According to Fig. 5, the average value of the dc bus voltage calculated by controllers after equalization can be expressed as follows:

$$\bar{v}_{\rm dc} = \frac{v_{\rm dc1} + v_{\rm dc2}}{2}. \tag{34}$$

After secondary control adjustment implemented and with equalization voltage-shifting amount Δv, combining (33) and (34), $v_{\rm avg}$ can be yielded as

$$\begin{aligned} \bar{v}_{\rm dc} &= \frac{v_{\rm dc}^* + \Delta v - r_{d1} \cdot i_{\rm dc1} + v_{\rm dc}^* + \Delta v - r_{d2} \cdot i_{\rm dc2}}{2} \\ &= v_{\rm dc}^* + \Delta v - \frac{r_{d1} \cdot i_{\rm dc1} + r_{d2} \cdot i_{\rm dc2}}{2}. \end{aligned} \tag{35}$$

When the system reaches steady state and the output currents of two converters are equal, the reference value of the droop coefficient can be obtained as

$$r^* \approx \bar{r}_{\rm dc} = \frac{r_{d1} + r_{d2}}{2}. \tag{36}$$

Combining (35) and (36), $\bar{v}_{{\rm dc}i}$ can be expressed as

$$\bar{v}_{{\rm dc}i} = v_{\rm dc}^* + \Delta v - r_{\rm ref} \cdot i_{{\rm dc}i}. \tag{37}$$

The above equation indicates that under the equalization of voltage-shifting regulation, the average bus voltage could eventually reach the setting value with voltage-shifting adjustment value equal to $r_{\rm ref} \cdot i_{{\rm dc}i}$. It should be noted that as the output terminal voltages $v_{\rm dc1}, v_{\rm dc2}$ are selected as the sample targets, when their average value is equal to the setting bus voltage, the actual value of dc bus voltage will be slightly less than the setting value because of the line impedances.

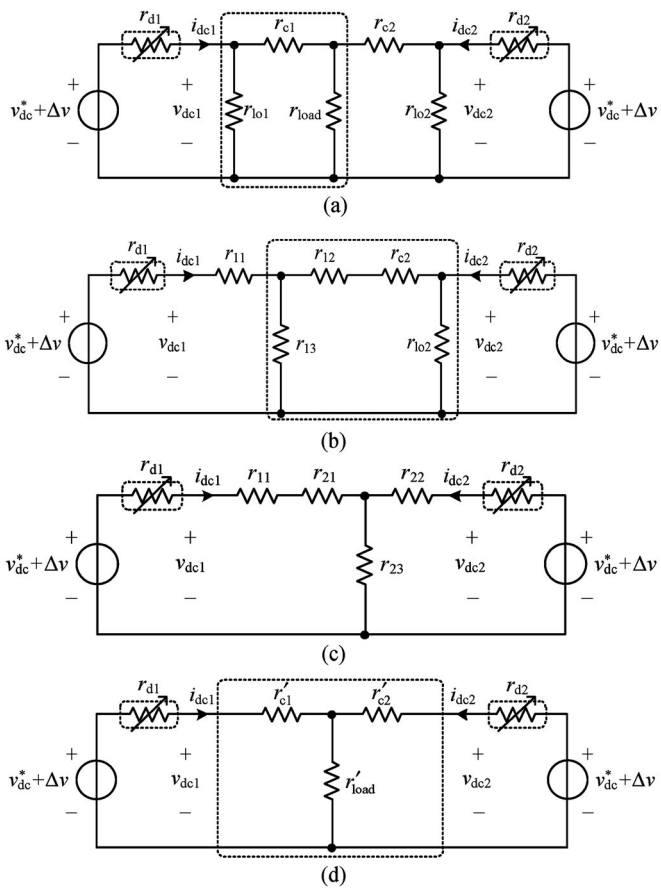

Fig. 8. Equivalent circuit of the proposed secondary control method considering both local loads and common load.

D. Analysis and Discussion of the Equivalent Circuit With Local Loads

Besides the common load connected at the PCC, local loads also usually exist in dc MGs, where the local loads, common loads, and line impedances form an impedance network. As shown in Fig. 8(a), the equivalent circuit model of the dc MG with two terminals can be derived, where $r_{\rm lo1}$ and $r_{\rm lo2}$ represent the two local loads connected at the output terminals of converter #1 and #2, and the impact of both local and common loads is taken into account.

It can be seen that a π-type impedance model comprised of $r_{\rm lo1}, r_{\rm cl}$ and $r_{\rm load}$ is formed in Fig. 8(a). By using Δ-Y transformation, the equivalent circuit model in Fig. 8(a) can be changed to Fig. 8(b). Here, r_{l1}, r_{l2} and r_{l3} in Fig. 8(b) can be derived as

$$\begin{cases} r_{11} = \dfrac{r_{c1} r_{lo1}}{r_{c1} + r_{lo1} + r_{\rm load}} \\ r_{12} = \dfrac{r_{c1} r_{\rm load}}{r_{c1} + r_{lo1} + r_{\rm load}} \\ r_{13} = \dfrac{r_{lo1} r_{\rm load}}{r_{c1} + r_{lo1} + r_{\rm load}} \end{cases}. \tag{38}$$

Meanwhile, by using Δ-Y transformation for the π-type impedance model comprised of $r_{13}, r_{12}, r_{c2}, r_{\rm lo2}$, Fig. 8(b) can

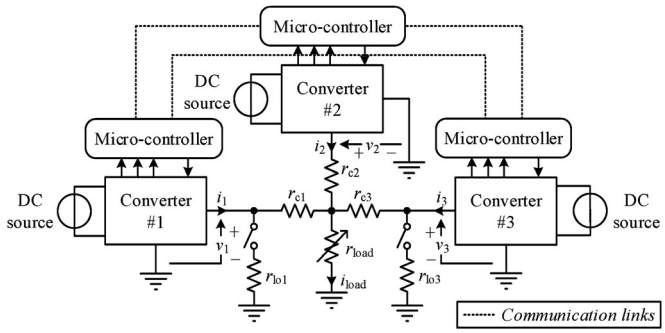

Fig. 9. Configuration of the prototype with three interface converters.

TABLE II
SYSTEM PARAMETERS

Parameters	Symbol	Value
Input voltage	$v_{\rm in}$	100 V
Reference value of output voltage	$v_{\rm ref}$	200 V
Power rating	$P_{\rm rate}$	1 kW
Switching frequency	$f_{\rm sw}$	20 kHz
Filter inductor	L_f	2 mH
Filter capacitor	C_f	470 uF
Droop coefficient	r_d	10 Ω

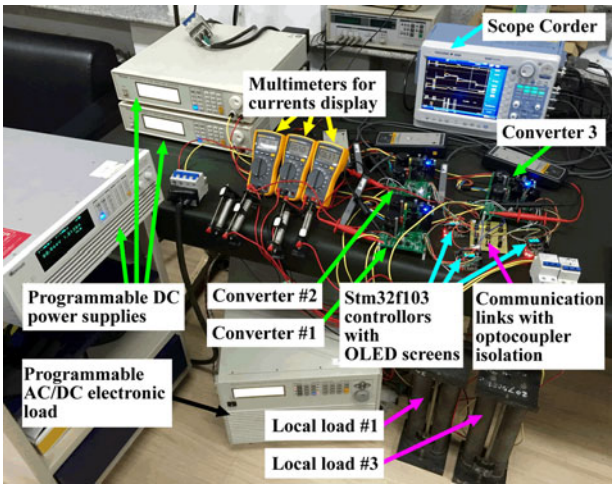

Fig. 10. Picture of the prototype.

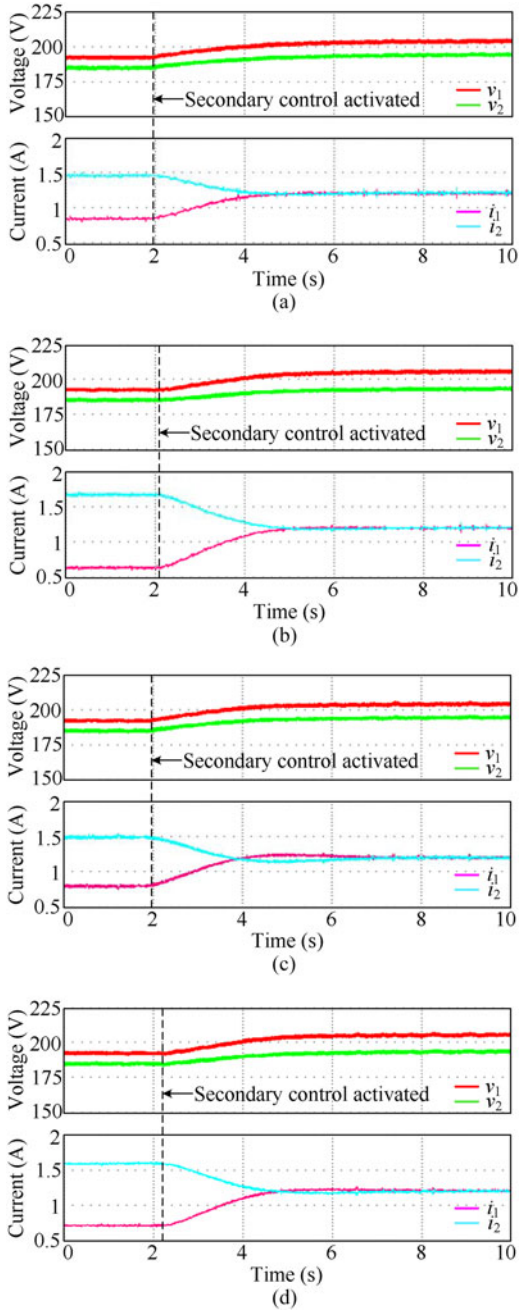

Fig. 11. Experimental results of the proposed method with different communication delays and line impedances ($R_{\rm load} = 80\,\Omega$): (a) communication delay: 300 ms, line impedances: 7.6 Ω, 0.4 Ω; (b) communication delay: 300 ms, line impedances: 15.3 Ω, 0.4 Ω; (c) communication delay: 600 ms, line impedances: 8.2 Ω, 0.4 Ω; (d) communication delay: 600 ms, line impedances: 12.7 Ω, 0.4 Ω.

be further changed to Fig. 8(c), where r_{21}, r_{22} and r_{23} can be derived as

$$\begin{cases} r_{21} = \dfrac{(r_{l2}+r_{c2})r_{13}}{r_{13}+r_{l2}+r_{c2}+r_{lo2}} \\ r_{22} = \dfrac{(r_{l2}+r_{c2})r_{lo2}}{r_{13}+r_{l2}+r_{c2}+r_{lo2}} \\ r_{23} = \dfrac{r_{13}r_{lo2}}{r_{13}+r_{l2}+r_{c2}+r_{lo2}} \end{cases}. \tag{39}$$

By combining the impedances in Fig. 8(c), a modified model considering both local and common loads can be obtained, where the equivalent line impedances and the equivalent common load are shown as

$$\begin{cases} r'_{\rm c1} = r_{11}+r_{21} \\ r'_{\rm c2} = r_{22} \\ r'_{\rm load} = r_{23} \end{cases}. \tag{40}$$

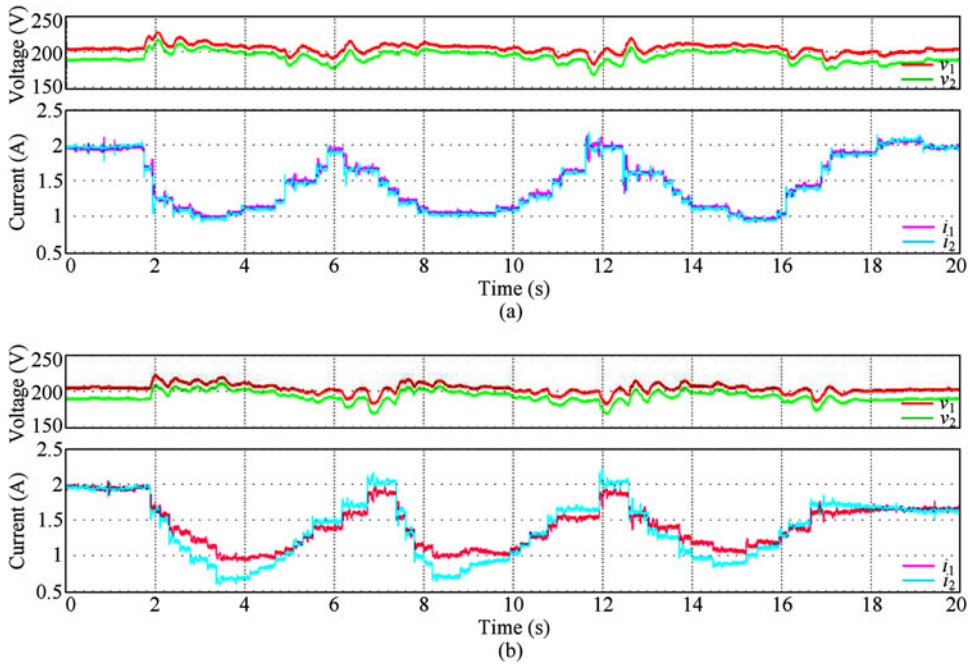

Fig. 12. Dynamic performance of the proposed method and voltage-shifting method (communication delay: 300 ms; line impedances: 8.2 Ω, 0.4 Ω): (a) proposed method with load fluctuations; (b) voltage-shifting method with load fluctuations.

Substituting (38) and (39) into (40) and assuming $R_{eq} = r_{c1} + r_{\rm lo1} + r_{\rm load}$, it yields

$$\begin{cases} r'_{c1} = \dfrac{r_{c1}r_{lo1}}{R_{eq}} + \dfrac{(r_{c1}r_{\rm load} + R_{eq}r_{c2})r_{lo1}r_{\rm load}}{r_{lo1}r_{\rm load} + r_{c1}r_{\rm load} + R_{eq}\left(r_{c2} + r_{lo2}\right)} \\ r'_{c2} = \dfrac{(r_{c1}r_{\rm load} + R_{eq}r_{c2})r_{lo2}}{r_{lo1}r_{\rm load} + r_{c1}r_{\rm load} + R_{eq}\left(r_{c2} + r_{lo2}\right)} \\ r'_{\rm load} = \dfrac{r_{lo1}r_{\rm load}r_{lo2}}{r_{lo1}r_{\rm load} + r_{c1}r_{\rm load} + R_{eq}\left(r_{c2} + r_{lo2}\right)} \end{cases}. \tag{41}$$

It can be seen from Fig. 8 and (38)–(41) that the dc MG with both local loads and common load can be equivalently changed to an impedance model with only common load and line impedances by using Δ-Y transformation. Hence, it can be concluded that even though local loads exist in dc MG, the equivalent system model in Fig. 5 can be also used. When the common or local load changes, the proposed secondary control diagram with average output current controller and average droop coefficient controller can dynamically adjust the droop coefficients and finally equalize the equivalent output impedances so that the desired load current sharing can be thereby achieved. By using the Thevenin equivalent circuit, the similar conclusion can be drawn with more than two parallel converters working together.

It should be noted that the values of local loads, common load, and line impedances are not used in the proposed secondary control diagram. The proposed method is realized by using the compensating controllers. The above circuit analysis is only used to theoretically study the effectiveness of the proposed method. Meanwhile, when the local loads change, the variations of the equivalent line impedances can be observed in (41). In some extreme cases, e.g., the practical line impedance is very large and the local load changes dramatically, the dynamic current sharing accuracy may be influenced due to the mismatched equivalent output impedances of the converters.

V. Experimental Verifications and Discussions

In order to validate the feasibility of the proposed secondary control method, a dc MG prototype is set up, as shown in Fig. 9. The dc MG setup is comprised of three boost converters, three dc power sources and dc loads to form an islanded dc MG. The dc loads consist of a common load and local loads. In particular, $r_{\rm load}$ is the common load connected at the PCC, and the local loads $r_{\rm lo1}, r_{\rm lo3}$ are connected at the output terminals of converter #1 and #3, respectively. The controllers of converters can communicate with each other via RS232 as an LBC network, and the converter parameters are listed in Table II.

A picture of the laboratory prototype is shown in Fig. 10. Multimeters (Fluke 115C) are used to observe the output currents of three converters; adjustable winding resistances are used as the line impedances; communication terminals are isolated by optocouplers; a programmable dc electronic load is used as the common load in the system; two slide resistances are used as local loads. The programmable dc electronic load is set at the resistance mode and its value can be altered in the host computer or directly regulated by using its control panel. Therefore, the fast-changing load condition can be emulated by regulating the resistance of the dc electronic load. The voltage and current inner control loops and secondary control algorithms are implemented by using STM32F103 MCU, which is a low-cost digital controller. The human–machine interface allows easy observation of the internal parameters of the system.

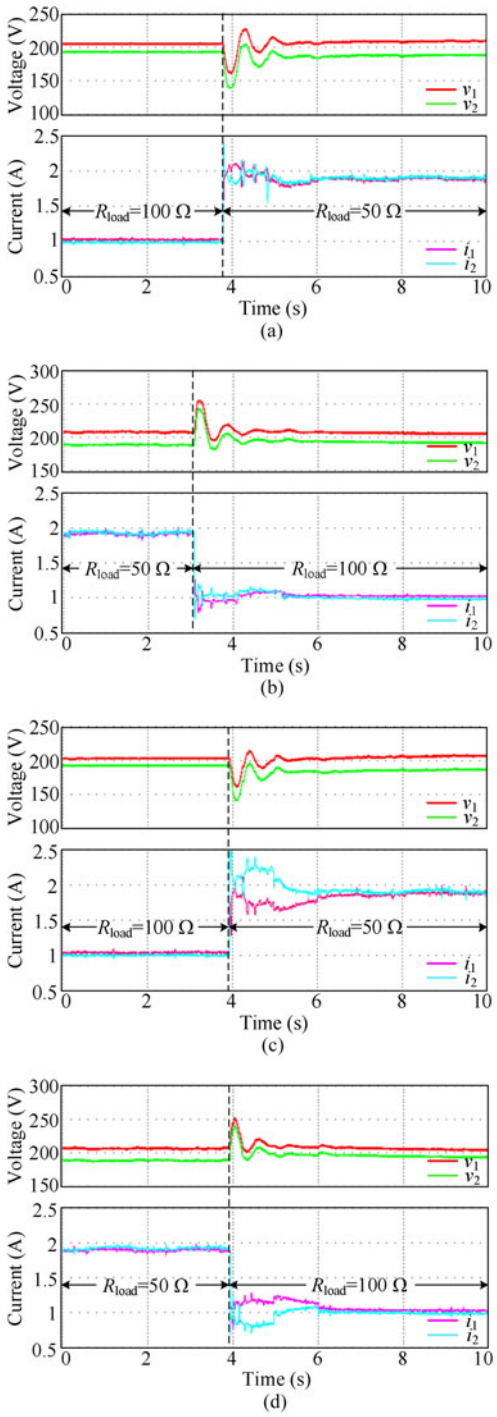

Fig. 13. Dynamic performance of the proposed method and voltage-shifting method (communication delay: 300 ms; line impedances: 8.2 Ω, 0.4 Ω): (a) proposed method with the sudden rise of load; (b) proposed method with the sudden drawdown of load; (c) voltage-shifting method with the sudden rise of load; (d) voltage-shifting method with the sudden drawdown of load.

Experiments are tested in following cases: Case A verifies the basic performance of proposed secondary control; Case B compares the dynamic performance of the proposed secondary control under load fluctuations and step load changes with voltage-shifting-based secondary control. Case C investigates the effectiveness of the proposed secondary control when

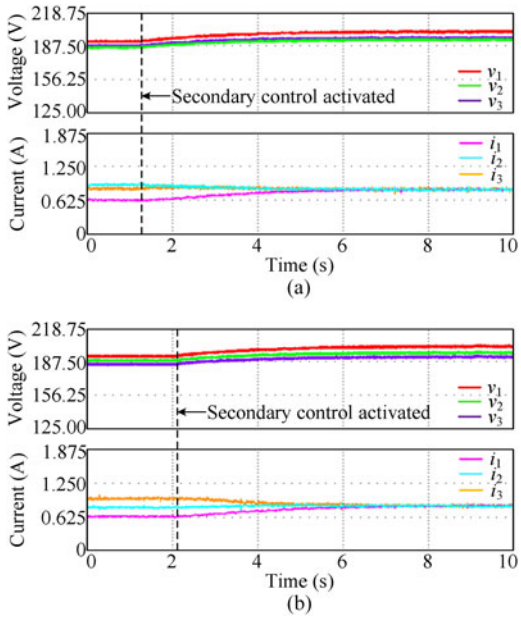

Fig. 14. Experimental results of the proposed method with different line impedances ($R_{\rm load} = 80\ \Omega$): (a) communication delay: 300 ms, line impedances: 8.3 Ω, 9.1 Ω, 1.7 Ω; (b) communication delay: 300 ms, line impedances: 8.3 Ω, 4.2 Ω, 1.7 Ω.

the three converters operate at the same time, and examines the validity of the proposed approach under the case when one of the converters fails and recovers from the failure after a period of time. Case D investigates the effectiveness of the proposed secondary control method when local loads are connected at the output terminals.

A. Case A. Basic Performance of the Proposed Secondary Control Method

In this section, two converters working in parallel are selected to test the proposed control method. The performance of the proposed secondary control with different communication delays and line impedances is investigated. As shown in Fig. 11, before the secondary control is activated, the output currents of two converters are not the same, and the error becomes larger when the difference between line impedances increases. When the secondary control is activated, the voltage deviations are eliminated, and the current sharing accuracy is significantly enhanced. The experimental results demonstrate the validity of the proposed LBC-based secondary control method, which can be used to maintain the current sharing accuracy with mismatched line impedances. It can be also seen from Fig. 11 that with larger communication delay, although secondary control works successfully, the regulating time becomes larger and the slight oscillation appears.

B. Case B. Dynamic Performance of the Proposed & Voltage-Shifting-Based Secondary Control Methods

Dynamic performance of the proposed secondary control compared to the conventional voltage-shifting method is

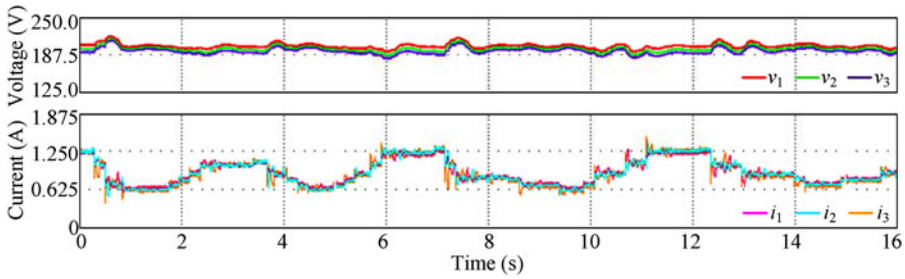

Fig. 15. Dynamic performance of the proposed method (communication delay: 300 ms; line impedances: 8.3 Ω, 4.2 Ω, 1.7 Ω).

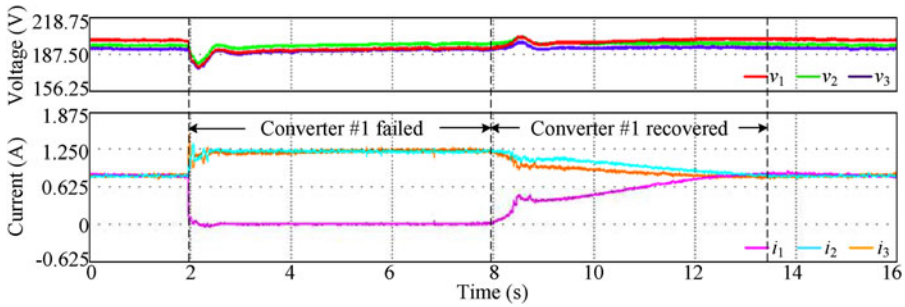

Fig. 16. Converter failure and recovery results of the proposed secondary control.

investigated under the condition of load fluctuations and load step. During the comparison, all the electrical and control parameters of converters are the same. As seen in Fig. 12(a) and (b), the proposed approach can still maintain a high current sharing accuracy under load fluctuations, whereas the dynamic performance of voltage-shifting method becomes poor.

In the conditions of load steps, the results of the proposed control approach are shown in Fig. 13(a) and (b). Compared to the results of voltage-shifting method shown in Fig. 13(c) and (d), the proposed approach features better current sharing transient response. This is because that the transient response of current sharing needs more time to adjust when load changes suddenly in voltage-shifting method since the equivalent output impedances are not the same.

C. Case C. Resilient Operation of Interface Converters With the Proposal Secondary Control Method

Furthermore, in order to validate the proposed secondary control in larger scale system and investigate the fault tolerant capability, three converters working in parallel are studied in this case. When three converters operate at the same time before the secondary control activated, as it can be seen from Fig. 14 that the output currents of the converters are not equal due to the mismatched line impedances. Meanwhile, when the difference of line impedances increases, the current sharing performance is further deteriorated. In contrast, with the proposed secondary control activated, the output currents of three converters maintain the same and dc bus voltage is restored successfully.

Fig. 15 shows the dynamic current sharing performance when three converters operating in parallel at the same time. It can be seen, when the load fluctuation occurs, the dynamic current sharing effect of the proposed secondary control is still satisfactory.

Additionally, the resiliency of the proposed algorithm is investigated when one of the converters fails for a period of time due to malfunction. From Fig. 16, it can be seen that at the beginning, with the proposed secondary control, the output currents of three converters are the same. Then converter #1 stops working due to malfunction and its output current drops to zero, while the load is continuously powered by converter #2 and #3. It can be seen that when converter #1 fails, the output currents of converter #2 and #3 increase rapidly and the current sharing accuracy is not influenced. When converter #1 recovers, with the proposed secondary control schemes, the output currents of three converters eventually become equal.

D. Case D. Test of the Proposed Secondary Control Method With Local Loads

In order to verify the effectiveness of the proposed secondary control method with the consideration of local loads, the performance of the system is tested when the local loads are connected or disconnected. As shown in Fig. 17, only a common load is connected and the load power is supplied by the three modules in the first stage. It can be seen that the output current of each converter is equalized by using the proposed method. In the second stage, the local load of converter #3, i.e., r_{lo3}, is connected. The output current of each converter increases due to the connection of r_{lo3}. Then, in the third stage, the local load of converter #1, i.e., r_{lo1}, is also connected. After a transient period, the output current of each converter can be equalized again with the proposed secondary control diagram. In the fourth and fifth stage, local loads r_{lo1} and r_{lo3} are disconnected sequentially. With the

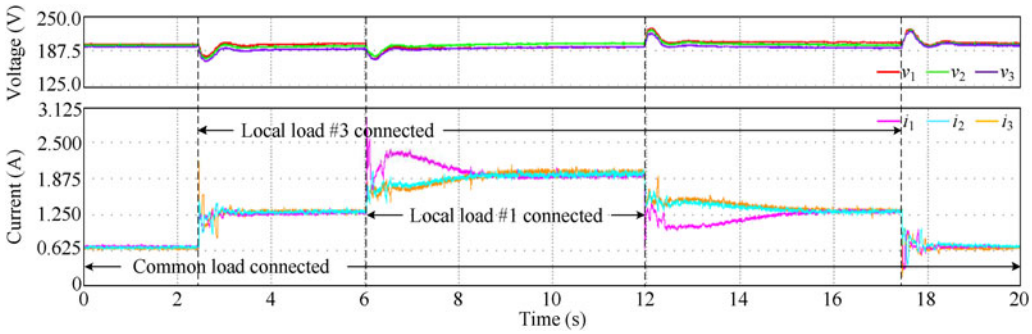

Fig. 17. Experimental results of the proposed method with local loads connected and disconnected ($r_{\rm load} = r_{\rm lo1} = r_{\rm lo3} = 100\ \Omega, r_{c1} = 8.3\ \Omega, r_{c2} = 4.2\ \Omega, r_{c3} = 1.7\ \Omega$).

common load and local loads existing together, it can be seen that the output current of each converter can be also equalized by using the proposed secondary control method.

It can be seen from Fig. 17 that when the local load of converter #3 is connected or disconnected, the transient current sharing accuracy is not significantly influenced. It is because that the line impedance connected to converter #3 is relatively small. Based on the derivation presented in Section IV-D, the equivalent line impedances with local load are similar to the real line impedances. Hence, no obvious influence of current sharing accuracy can be found. As also mentioned in Section IV-D, when the local load of converter #1 is connected, since the equivalent line impedance of converter #1 is relatively larger and the difference between the equivalent line impedances with the local loads and the real line impedances is larger, longer adjusting time can be seen in the waveforms. However, even though the transient time is longer, the desired current sharing accuracy can be still guaranteed by using the proposed secondary control diagram. Meanwhile, although the output current of converter #1 bias from its steady-state value during the transient period when considering the connection of the local load, high current sharing accuracy between converter #2 and #3 can be still maintained in all stages.

VI. Conclusion

This paper proposes an improved LBC-based distributed secondary control scheme for droop-controlled dc MG. Unlike conventional voltage-shifting-based secondary control methods, the current sharing accuracy is enhanced by using the additional average current controller and average droop coefficient controller. Hence, the equivalent output impedance can be equalized and the dynamic performance of the secondary control diagram with fast-changing load current can be thereby improved. Meanwhile, the average value of droop coefficients is calculated and regulated to reach the set value in the secondary control diagram to avoid the uncertain droop coefficients. Furthermore, the voltage-shifting equalization is employed to ensure the same voltage-shifting amounts of converters under distributed secondary control during the restoration of dc bus voltage. As a result, although LBC is employed for data exchanging in this method, desired proportional load sharing can be achieved in both steady state and transient conditions. Experimental results show that a better dynamic current sharing performance is achieved based on the proposed method. Meanwhile, test scenarios with converter failure and recovery show that the proposed secondary control scheme can ensure stable operation of the system. With the consideration of local loads, the proposed secondary control method is still valid to improve the current sharing accuracy since it is demonstrated that the dc MG with local loads can be changed to an equivalent system with common load only. Furthermore, the proposed control method is easy to execute in the low-cost digital controller, e.g., MCU, which is suitable for practical industrial applications.

References

[1] R. Lasseter, A. Akhil, C. Marnay, J. Stevens, J. Dagle, R. Guttromson, A. Meliopoulous, R. Yinger, and J. Oto, "The certs microgrid concept—White paper on integration of distributed energy resources," U.S. Dept. Energy, Lawrence Berkeley Nat. Lab., Berkeley, CA, USA, Tech. Rep. LBNL-50829, 2002.

[2] H. Kakigano, Y. Miura, and T. Ise, "Low-voltage bipolar-type dc microgrid for super high quality distribution," *IEEE Trans. Power Electron.*, vol. 25, no. 12, pp. 3066–3075, Dec. 2010.

[3] T. Dragičević, X. Lu, J. C. Vasquez, and J. M. Guerrero, "DC Microgrids–Part II: A review of power architectures, applications and standardization issues," *IEEE Trans. Power Electron.*, to be published.

[4] P. Cairoli, I. Kondratiev, and R. A. Dougal, "Coordinated control of the bus tie switches and power supply converters for fault protection in DC microgrids," *IEEE Trans. Power Electron.*, vol. 28, no. 4, pp. 2037–2047, Apr. 2013.

[5] Y. K. Chen, Y. C. Wu, C. C. Song, and Y. S. Chen, "Design and implementation of energy management system with fuzzy control for DC microgrid systems," *IEEE Trans. Power Electron.*, vol. 28, no. 4, pp. 1563–1570, Apr. 2013.

[6] L. Meng, T. Dragicevic, J. M. Guerrero, and J. C. Vasquez, "Dynamic consensus algorithm based distributed global efficiency optimization of a droop controlled DC microgrid," in *Proc. IEEE Int. Eng. Conf.*, 2014, pp. 1276–1283.

[7] J. Li, J. Su, X. Yang, and T. Zhao, "Study on microgrid operation control and black start," in *Proc. Elec. Utility Deregulation Restruct. Power Tec. Conf.*, 2011, pp. 1652–1655.

[8] J. Lee, B. Han, and H. Cha, "Development of hardware simulator for DC micro-grid operation analysis," in *Proc. IEEE Power Energy Soc. Gen. Meet.*, 2012, pp. 1–8.

[9] A. Khorsandi, M. Ashourloo, and H. Mokhtari, "A decentralized control method for a low-voltage DC microgrid," *IEEE Trans. Energy Convers.*, vol. 29, no. 4, pp. 793–801, Dec. 2014.

[10] T. Dragičević, X. Lu, J. C. Vasquez, and J. M. Guerrero, "DC microgrids–Part I: A review of control strategies and stabilization techniques," *IEEE Trans. Power Electron.*, to be published.

[11] D. Chen, L. Xu, and L. Yao, "DC voltage variation based autonomous control of DC microgrids," *IEEE Trans. Power Del.*, vol. 28, no. 2, pp. 637–648, Apr. 2013.

[12] D. Salomonsson, L. Soder, and A. Sannino, "An adaptive control system for a DC microgrid for data centers," *IEEE Trans. Ind. Appl.*, vol. 44, no. 6, pp. 1910–1917, Nov./Dec. 2008.
[13] L. Che and M. Shahidehpour, "DC microgrids: Economic operation and enhancement of resilience by hierarchical control," *IEEE Trans. Smart Grid*, vol. 5, no. 5, pp. 2517–2526, Sep. 2014.
[14] Q. Shafiee, T. Dragicevic, J.C. Vasquez, and J. M. Guerrero, "Hierarchical control for multiple DC-microgrids clusters," *IEEE Trans. Energy Convers.*, vol. 29, no. 4, pp. 922–933, Dec. 2014.
[15] C. Lin, P. Wang, J. Xiao, Y. Tang, and F. H. Choo, "Implementation of hierarchical control in DC microgrids," *IEEE Trans. Ind. Electron.*, vol. 61, no. 8, pp. 4032–4042, Aug. 2014.
[16] J. Shi, L. Zhou, and X. He, "Common-duty-ratio control of input-parallel output-parallel (IPOP) connected DC–DC converter modules with automatic sharing of currents," *IEEE Trans. Power Electron.*, vol. 27, no. 7, pp. 3277–3291, Jul. 2012.
[17] R. Ayyanar, R. Giri, and N. Mohan, "Active input-voltage and load-current sharing in input-series and output-parallel connected modular DC-DC converters using dynamic input-voltage reference scheme," *IEEE Trans. Power Electron.*, vol. 19, no. 6, pp. 1462–1473, Nov. 2004.
[18] J. M. Guerrero, L. D. Vicuna, J. Matas, J. Miret, and J. Cruz, "Steady-state invariant frequency and amplitude droop control using adaptive output impedance for parallel-connected UPS inverters," in *Proc. Appl. Power Elec. Conf. Exp.*, 2005, pp. 560–566.
[19] Z. Ye, D. Boroyevich, K. Xing, and F. C. Lee, "Design of parallel sources in DC distributed power systems by using gain-scheduling technique," in *Proc. Power Elec. Spec. Conf.*, 1999, pp. 161–165.
[20] K. Siri and J. Banda, "Current distribution for parallel-connected DC power sources without remote sensing," in *Proc. Telecom. Energy Conf.*, 1994, pp. 196–203.
[21] Z. Moussaoui, I. Batarseh, H. Lee, and C. Kennedy, "An overview of the control scheme for distributed power systems," in *Proc. Southcon Conf. Rec.*, 1996, pp. 584–591.
[22] T. Dragicevic, J. Guerrero, J. Vasquez, and D. Skrlec, "Supervisory control of an adaptive-droop regulated dc microgrid with battery management capability," *IEEE Trans. Power Electron.*, vol. 29, no. 2, pp. 695–706, Feb. 2014.
[23] P. Huang, W. Xiao, and M. S. Moursi, "A practical load sharing control strategy for DC microgrids and DC supplied houses," in *Proc. 39th Annu. Conf. IEEE Ind. Electron. Soc.*, 2013, pp. 7122–7126.
[24] A. P. N. Tahim, D. J. Pagano, E. Lenz, and V. Stramosk, "Modeling and stability analysis of islanded DC microgrids under droop control," *IEEE Trans. Power Electron.*, vol. 30, no. 8, pp. 4597–4607, Aug. 2015.
[25] Y. Gu, X. Xiang, W. Li, and X. He, "Mode-adaptive decentralized control for renewable DC microgrid with enhanced reliability and flexibility," *IEEE Trans. Power Electron.*, vol. 29, no. 9, pp. 5072–5080, Sep. 2014.
[26] J. Beerten and R. Belmans, "Analysis of power sharing and voltage deviations in droop-controlled DC grids," *IEEE Trans. Power Syst.*, vol. 28, no. 4, pp. 4588–4597, Nov. 2013.
[27] J. M. Guerrero, J. Vasquez, J. Matas, L. de Vicuna, and M. Castilla, "Hierarchical control of droop-controlled ac and dc microgrids a general approach toward standardization," *IEEE Trans. Ind. Electron.*, vol. 58, no. 1, pp. 158–172, Jan. 2011.
[28] S. Anand, B. G. Fernandes, and J. M. Guerrero, "Distributed control to ensure proportional load sharing and improve voltage regulation in low voltage DC microgrids," *IEEE Trans. Power Electron.*, vol. 28, no. 4, pp. 1900–1913, Apr. 2013.
[29] X. Lu, J. M. Guerrero, K. Sun, and J. Vasquez, "An improved droop control method for dc microgrids based on low bandwidth communication with dc bus voltage restoration and enhanced current sharing accuracy," *IEEE Trans. Power Electron.*, vol. 29, no. 4, pp. 1800–1812, Apr. 2014.
[30] V. Nasirian, S. Moayedi, A. Davoudi, and F. L. Lewis, "Distributed cooperative control of DC microgrids," *IEEE Trans. Power Electron.*, vol. 30, no. 4, pp. 2288–2303, Apr. 2015.
[31] V. Nasirian, A. Davoudi, F. L. Lewis, and J. M. Guerrero, "Distributed adaptive droop control for DC distribution systems," *IEEE Trans. Energy Convers.*, vol. 29, no. 4, pp. 944–956, Dec. 2014.
[32] Q. Shafiee, J. M. Guerrero, and J. C. Vasquez, "Distributed secondary control for islanded microgrids—A novel approach," *IEEE Trans. Power Electron.*, vol. 29, no. 2, pp. 1018–1031, Feb. 2014.
[33] X. Yu, X. She, and A. Huang, "Hierarchical power management for DC microgrid in islanding mode and solid state transformer enabled mode," in *Proc. 39th Annu. Conf. IEEE Ind. Electron. Soc.*, 2013, pp. 1656–1661.
[34] H. Han, Y. Liu, Y. Sun, M. Su, and J. M. Guerrero, "An improved droop control strategy for reactive power sharing in islanded microgrid," *IEEE Trans. Power Electron.*, vol. 30, no. 6, pp. 3133–3141, Jun. 2015.
[35] S. K. Mazumder, M. Tahir, and K. Acharya, "Master–slave current-sharing control of a parallel DC–DC converter system over an RF communication interface," *IEEE Trans. Ind. Electron.*, vol. 55, no. 1, pp. 59–66, Jan. 2008.
[36] S. K. Mazumder, K. Acharya, and M. Tahir, "Joint optimization of control performance and network resource utilization in homogeneous power networks," *IEEE Trans. Ind. Electron.*, vol. 56, no. 5, pp. 1736–1745, May 2009.
[37] K. Acharya, M. Tahir, and S. K. Mazumder, "Communication fault-tolerant wireless network control of a load-sharing multiphase interactive power network," in *Proc. IEEE Power Elec. Spec. Conf.*, 2006, pp. 1167–1174.
[38] B. Wang, M. Sechilariu, and F. Locment, "Intelligent DC microgrid with smart grid communications: Control strategy consideration and design," *IEEE Trans. Smart Grid*, vol. 3, no. 4, pp. 2148–2156, Dec. 2012.
[39] X. Lu, K. Sun, J. M. Guerrero, J. C. Vasquez, and L. Huang, "State-of-charge balance using adaptive droop control for distributed energy storage systems in DC microgrid applications," *IEEE Trans. Ind. Electron.*, vol. 61, no. 6, pp. 2804–2815, Jun. 2014.
[40] S. Augustine, M. K. Mishra, and N. Lakshminarasamma, "Adaptive droop control strategy for load sharing and circulating current minimization in low-voltage standalone DC microgrid," *IEEE Trans. Sustain. Energy*, vol. 6, no. 1, pp. 132–141, Jan. 2015.

Panbao Wang (S'10–M'11) received the M.S. degree in electrical engineering from the Harbin Institute of Technology, Harbin, China, in 2011, where he is currently working toward the Ph.D. degree.

His research interests include dc microgrid system model analysis, operation and control, power electronics converters for hybrid storage system, and optimal control for power management in microgrid system, etc.

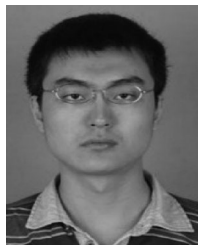

Xiaonan Lu (S'11–M'14) was born in Tianjin, China, in 1985. He received the B.E. and Ph.D. degrees in electrical engineering from Tsinghua University, Beijing, China, in 2008 and 2013, respectively. From September 2010 to August 2011, he was a guest Ph.D. student at the Department of Energy Technology, Aalborg University, Denmark.

From October 2013 to December 2014, he was a Postdoc Researcher in the Department of Electrical Engineering and Computer Science, University of Tennessee, Knoxville, TN, USA. In January 2015, he joined the Energy Systems Division, Argonne National Laboratory, where he is currently a Postdoc Appointee. His research interests include modeling and control of power electronic converters in renewable energy systems and microgrids, hardware-in-the-loop real-time simulation, active distribution system, multilevel converters, matrix converters, etc.

Dr. Lu cochaired the special session entitled DC Microgrids: Control, Operation and Trends in IEEE Energy Conversion Congress and Exposition in 2015. He received the Outstanding Reviewer Award for IEEE Transaction on Power Electronics in 2014. He is a Member of the IEEE PELS, IAS, and PES Society.

Xu Yang was born in Hohhot, Inner Mongolia, in 1991. He received the B.E. degree in electrical engineering from Southwest Jiaotong University, Chengdu, China, in 2014. He is currently working toward the M.S. degree in power electronics from the Harbin Institute of Technology, Harbin, China.

His research interests include dc microgrids, multiport dc/dc converter and power conversion for hybrid electric vehicle, electric vehicle, and fuel cell vehicle.

Wei Wang was born in Heilongjiang Province, China, in 1963. She received the B.S. degrees in automatic test and control from the Harbin Institute of Technology, Harbin, China, in 1984, the M.S. degree in electrical engineering from the Harbin Institute of Technology, Harbin, China, in 1990, and the Ph.D. degree in mechanical electronic engineering from the Harbin Institute of Technology, in 2002.

Since 2003, she has been a Professor with the Department of Electrical Engineering, Harbin Institute of Technology. She is engaged in research on soft-switching converters, photovoltaic grid-connected inverters, and AC & DC microgrids technique.

Dianguo Xu (M'97–SM'12) received the B.S. degree in control engineering from Harbin Engineering University, Harbin, China, in 1982, and the M.S. and Ph.D. degrees in electrical engineering from the Harbin Institute of Technology (HIT), Harbin, China, in 1984 and 1989, respectively.

In 1984, he joined the Department of Electrical Engineering, HIT as an Assistant Professor. Since 1994, he has been a Professor in the Department of Electrical Engineering, HIT. He was the Dean of School of Electrical Engineering and Automation, HIT from 2000 to 2010. He is currently the Vice President of HIT. His research interests include renewable energy generation technology, multiterminal HVDC system based on VSC, power quality mitigation, speed sensorless vector controlled motor drives, high-performance PMSM servo system. He published more than 600 technical papers.

Prof. Xu is an Associate Editor of the IEEE TRANSACTIONS ON INDUSTRIAL ELECTRONICS and the IEEE JOURNAL OF EMERGING AND SELECTED TOPICS IN POWER ELECTRONICS. He also serves as Chairman of IEEE Harbin Section, Director of Lighting Power Supply Committee of CPSS, Vice-director of Electric Automation Committee of CAA, Electrical Control System & Equipment Committee of CES, and Power Electronics Committee of CES.